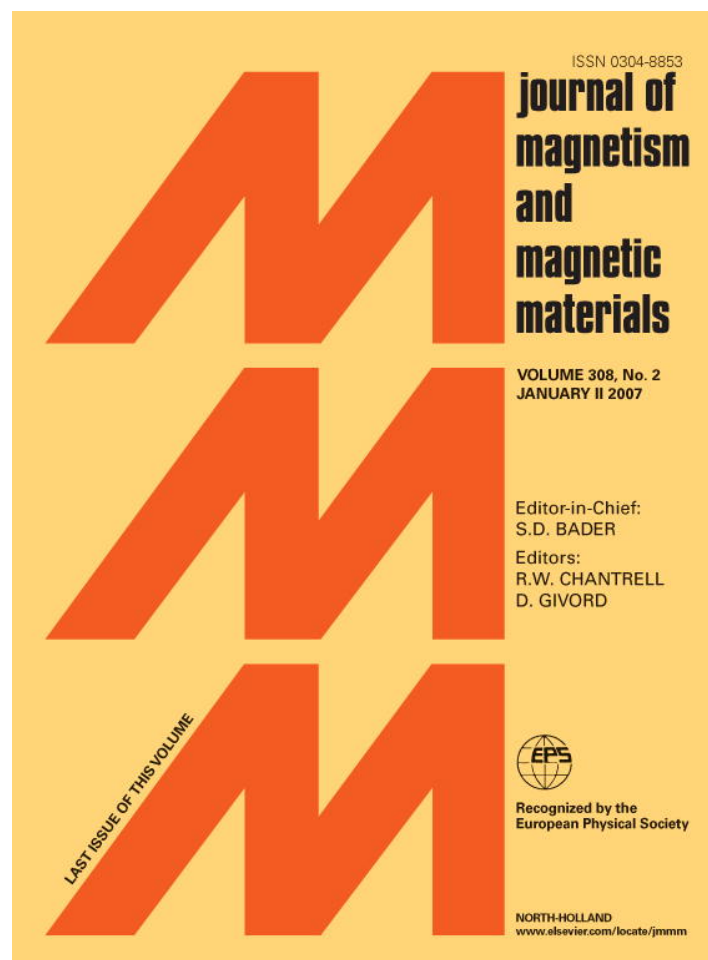


Provided for non-commercial research and educational use only.
Not for reproduction or distribution or commercial use.



This article was originally published in a journal published by Elsevier, and the attached copy is provided by Elsevier for the author's benefit and for the benefit of the author's institution, for non-commercial research and educational use including without limitation use in instruction at your institution, sending it to specific colleagues that you know, and providing a copy to your institution's administrator.

All other uses, reproduction and distribution, including without limitation commercial reprints, selling or licensing copies or access, or posting on open internet sites, your personal or institution's website or repository, are prohibited. For exceptions, permission may be sought for such use through Elsevier's permissions site at:

<http://www.elsevier.com/locate/permissionusematerial>

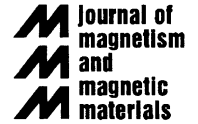


ELSEVIER

Available online at www.sciencedirect.com

ScienceDirect

Journal of Magnetism and Magnetic Materials 308 (2007) 233–237



www.elsevier.com/locate/jmmm

Phase diagrams of magnetic nanotubes

J. Escrig^a, P. Landeros^a, D. Altbir^a, E.E. Vogel^b, P. Vargas^{c,*}

^a*Departamento de Física, Universidad de Santiago de Chile, USACH, Av. Ecuador 3493, Santiago, Chile*

^b*Departamento de Ciencias Físicas, Universidad de la Frontera, Casilla 54-D, Temuco, Chile*

^c*Departamento de Física, Universidad Técnica Federico Santa María, Casilla 110-V, Valparaíso, Chile*

Received 24 December 2005; received in revised form 29 April 2006

Available online 19 June 2006

Abstract

Analytical expressions for the total magnetic energy of two characteristic internal configurations of nanometric tubes are calculated. A magnetic phase diagram with respect to the aspect ratio of the tubes is obtained which allows a discussion about the possibility of getting ensembles of nanotubes with low coercive fields. A comparison with recently reported coercive fields of three different cobalt nanotube arrays agrees well with the phase diagram derived here.

© 2006 Elsevier B.V. All rights reserved.

Keywords: Magnetic nanotubes; Phase diagrams

1. Introduction

In recent years, a great deal of attention has been focused on the study of regular arrays of magnetic particles. Besides the basic scientific interest in the magnetic properties of these systems, there is evidence that they might be used in the production of new magnetic devices, or as media for high density magnetic recording [1]. One of the main points in the study of such systems concerns the internal magnetic structure of the nanoparticles as a function of their shape and size. For example, in the case of cylindrically shaped particles produced by electrodeposition, the internal arrangements of the magnetic moments have been identified as close to one of the following three (idealized) characteristic configurations, namely perpendicular with the magnetization perpendicular to the cylinder axis ($F1$), parallel with the magnetization parallel to the cylinder axis ($F2$), and a vortex state, in which most of the magnetic moments lie parallel to the basis of the cylinder (V) [2,3]. The occurrence of each of these configurations depends on geometrical factors, such as the linear dimensions of the cylinders and their aspect ratio. Clearly, for the development of magnetic devices based on those

arrays, knowledge of the internal magnetic structure of the particles is of fundamental importance. Very recently [4], the synthesis of arrays of composite magnetic nanotubes formed in porous alumina has been reported. The thin-walled cobalt nanotubes are coated with a polymer layer on their inner walls. The composite nature of the magnetic tubes may be suitable for applications in biotechnology, where magnetic nanostructures with low density, which can float in solutions, are very desirable. In the leading paper by Nielsch et al. [4] three different aspect ratios are considered, showing different behaviors, which encourage a study about the possible magnetic phases or configurations in the nanotubes. Due to the very narrow hysteresis loops that are obtained, such phases are not easily identifiable from magnetization curves, and then a theoretical or numerical study can shine light on this problem.

A theoretical study based on a discrete distribution of magnetic moments would be extremely time consuming or eventually impossible using present standard computational facilities. The reason is the exceedingly large number of magnetic moments within such nanotubes, which may exceed 10^{10} . With this in mind, in this paper we adopt a continuous model for the internal magnetic structure of the particles, on the basis of which analytical results for the total energy in each configuration can be obtained. We will

*Corresponding author.

E-mail address: patricio.vargas@usm.cl (P. Vargas).

present an analytical expression for the line separating the vortex from a parallel phase, as a function of geometrical parameters.

2. Continuous magnetization model

We adopt a simplified description of the system, in which the discrete distribution of magnetic moments is replaced by a continuous one characterized by the magnetization $\vec{M}(\vec{r})$, such that $\vec{M}(\vec{r})\delta V$ gives the total magnetic moment within the element of volume δV centered at \vec{r} . This model provides a fairly good basis for the discussion of the magnetic properties of nanosized particles.

The internal magnetic energy, E_{tot} , of a single tube is given by the sum of three terms corresponding to the magnetostatic (E_{dip}), the exchange (E_{ex}), and the anisotropy (E_{K}) contributions. Our model does not consider crystallographic anisotropy which is appropriate for polycrystalline systems. In polycrystalline particles usually the crystallographic orientations of the crystallites are random and, as a consequence, the average magnetic anisotropy of the particle is very small. Then it is usually disregarded [5,6]. Because the nanotubes motivating this work are polycrystalline [4] we will not consider anisotropy in our model. Additionally, we have to recall that in these systems the main anisotropy is the shape anisotropy originating in the dipolar interactions within the tube. The dipolar contribution can be obtained from the knowledge of the magnetization, namely:

$$E_{\text{dip}} = \frac{\mu_0}{2} \int_V \vec{M}(\vec{r}) \cdot \nabla U(\vec{r}) dv, \quad (1)$$

where the magnetostatic potential is given by

$$U(\vec{r}) = \frac{\gamma_{\text{B}}}{4\pi} \int_S \frac{\vec{n}' \cdot \vec{M}(\vec{r}')}{|\vec{r} - \vec{r}'|} ds' - \frac{\gamma_{\text{B}}}{4\pi} \int_V \frac{\nabla \cdot \vec{M}(\vec{r}')}{|\vec{r} - \vec{r}'|} dv'. \quad (2)$$

In the previous expression, the first integral runs over the surface of the nanotube, while the second term integrates over the volume, with \vec{n}' a unit vector successively perpendicular to each of the four portions of the surface. Here γ_{B} is the Brown factor [7], namely, 1 in the International System of units, which we adopt from now on. The geometrical parameters defining the cylindrical nanotube are the following: height (or length) H ; external radius R ; internal radius a ; ratios $\beta = a/R$ and $\gamma = H/R$. Thus the full cylinder condition corresponds to $\beta = 0.0$ while our interest is focused on systems defined by β close to 1.0.

Assuming that the magnetization varies slowly on the scale of the lattice parameter, the exchange energy of the particle can be added by means of the following expression [7]:

$$E_{\text{ex}} = A \int_V ((\nabla m_x)^2 + (\nabla m_y)^2 + (\nabla m_z)^2) dv, \quad (3)$$

where $m_i = M_i/M_0$ is the normalized component of the magnetization with respect to the saturation magnetization M_0 ; A is the stiffness constant of the material, which is

proportional to the exchange constant between pairs of magnetic atoms. We are leaving out of the right-hand side a constant term which is independent of the magnetic configuration [7].

To go on with the calculations we need to make assumptions on the nature of possible magnetization configurations discussed in the introduction. For long nanowires ($\gamma \gg 1$), the $F1$ phase is not present [8], a result that holds for nanotubes also [9]. For the $F2$ parallel phase, from now on just F , we can make the assumption of homogeneity, namely, $\vec{M}(\vec{r}) = M_0 \hat{z}$ with \hat{z} a unit vector parallel to the axis of the nanotube.

For the vortex configuration, V , we assume that the magnetization has the general form (including a magnetic core)

$$\vec{M}(\vec{r}) = M_z(r)\hat{z} + M_\phi(r)\hat{\phi}, \quad (4)$$

where \hat{z} and $\hat{\phi}$ are unit vectors in cylindrical coordinates, and M_z (component responsible for the core magnetization) and M_ϕ (component giving the true vortex magnetization) satisfy the relation $M_z^2 + M_\phi^2 = M_0^2$.

The question arises whether a core exists for a cylinder with sufficiently large inner radius. In order to clarify this point micromagnetic simulations of the state of minimum energy have been computed by means of the OOMMF package [10]. To mimic experimental results [4] we used the following parameters for hcp cobalt [11] in the reported nanotubes: $M_0 = 1.4 \times 10^6$ A/m, stiffness constant $A = 1 \times 10^{-11}$ J/m and choose cubic cells of $4.0 \times 4.0 \times 10.0$ nm³. Simulations were done for different β values and we found that for tubes with thin walls the core becomes negligible. In Fig. 1 we present the results of two simulations: (a) for $\beta = 0.1$, and (b) for $\beta = 0.3$. Arrows represent the ϕ component of the magnetization; then, a short arrow in this diagram means that there is a magnetization component along the z direction thus producing a core. For $\beta = 0.1$ the ratio $M_z/M_0 = 0.11$, while for $\beta = 0.3$, $M_z/M_0 \approx 10^{-6}$. From these results we can conclude that, generally speaking, for $\beta > 0.3$ the core can be safely disregarded. Since the experimental work considered very narrow tubes (β close to 1.0), we will neglect the effect of the core from now on. In such case

$$\vec{M}(\vec{r}) = M_0 \hat{\phi}. \quad (5)$$

We then look at the total energy of both configurations under consideration, F and V , from which the magnetic phase diagram can be obtained. The transition line is obtained upon equating the expressions for the energy in both configurations. We restrict our discussion to arrays in which the separation between tubes is sufficiently large for the interaction between them to be ignored.

2.1. Parallel configuration

From Eqs. (1) and (2) and by expanding $|r - r'|^{-1}$ we can obtain the following expression for the dipolar contribu-

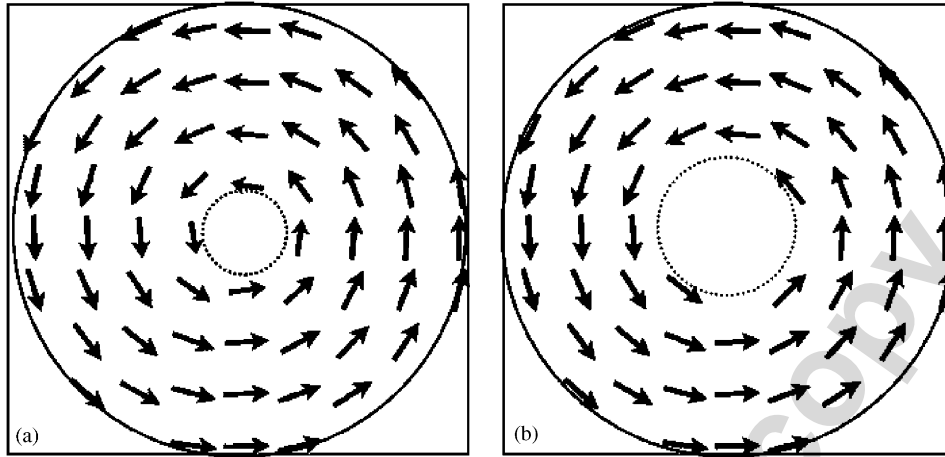


Fig. 1. Snapshots of the magnetization along a plane perpendicular to the tube axis. The size of the arrows gives the magnitude of the component of the in-plane magnetization. The nanotube is defined by $R = 52$ nm, $H = 700$ nm and (a) $\beta = 0.1$ ($M_z/M_0 = 0.11$), and (b) $\beta = 0.3$ ($M_z/M_0 \approx 10^{-6}$).

tion to the energy in the parallel configuration

$$E_{\text{dip}}^F = \pi\mu_0 M_0^2 R^3 \int_0^\infty \frac{1 - e^{-\gamma y}}{y^2} (J_1(y) - \beta J_1(\beta y))^2 dy. \quad (6)$$

In this expression $J_1(z)$ are Bessel functions of first order and first kind. Some terms in this equation can be expressed as hypergeometric functions and one term requires numerical calculation for its evaluation.

From Eq. (3) it follows that $E_{\text{ex}}^F = 0$.

2.2. Vortex configuration

The dipolar energy in the vortex configuration is equal to zero as it follows by evaluation of Eq (2). Upon combining Eqs. (3) and (5) we find

$$E_{\text{ex}}^V = 2\pi H A \ln \frac{1}{\beta}. \quad (7)$$

In Fig. 2, we illustrate the reduced energy of both configurations, vortex and parallel, as a function of β for $H/L_x = 5000$ and $R/L_x = 25$, being L_x the exchange length of the material defined by $L_x = \sqrt{2A/\mu_0 M_0^2}$. These dimensions are representative of the experimental points *a, b* and *c* illustrated in Fig. 3. For these nanotube parameters we note that there are two transition points corresponding approximately to $\beta \approx 0.4$ and $\beta \approx 0.68$. Within these two values, the vortex state is preferred. If we slightly diminish the radius, the two transition points collapse in one corresponding to $\beta \approx 0.55$. For smaller values of R/L_x no transition point is found, and only the parallel state is the most stable.

2.3. Phase diagram and discussion

To obtain an expression for the transition line separating the parallel phase from the vortex phase we match the

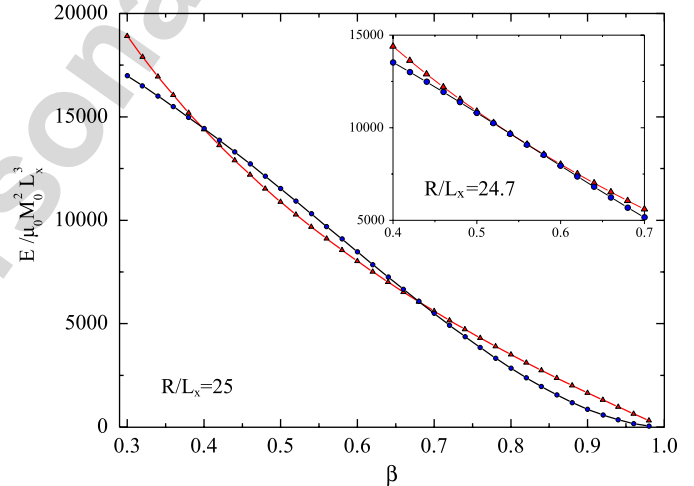


Fig. 2. Magnetic energy of the parallel (circles) and vortex (triangles) configurations of a tube in units of $\mu_0 M_0^2 L_x^3$, as a function of β . The dimensions of the tube are $H/L_x = 5000$ and $R/L_x = 25$. Inset shows results for same H/L_x and $R/L_x = 24.47$.

expressions for the energy of these two configurations given by Eqs. (6) and (7), respectively. This leads to the following condition:

$$\frac{h}{r^3} = \frac{1}{\ln 1/\beta} \int_0^\infty \frac{1 - e^{-\gamma y}}{y^2} (J_1(y) - \beta J_1(\beta y))^2 dy, \quad (8)$$

where $h \equiv H/L_x$ and $r \equiv R/L_x$. The argument of the integral of Eq. (8) tends to zero as $y \rightarrow 0$, which allows to neglect the term $e^{-\gamma y}$ in the numerator, since it would be important only around $y = 0.0$. This is especially reinforced for the large values of γ under consideration. Then we bring out approximate analytical expressions for the transition condition in terms of the ratio β of the nanotube:

$$\frac{h}{r^3} = \frac{1}{\ln 1/\beta} \left(\frac{4}{3\pi} (1 + \beta^3) - \beta^2 F_{21}[\beta] \right) \equiv \alpha(\beta), \quad (9)$$

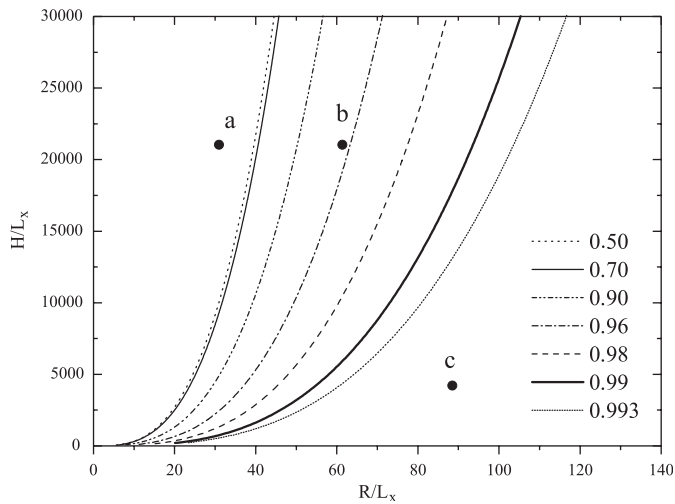


Fig. 3. Magnetic phase diagrams of non-interacting nanotubes for different values of β within the range $[0.50, 0.993]$. The dimensions of the tube, H and R , are normalized to the exchange length L_x . Experimental points a, b and c are discussed in the text.

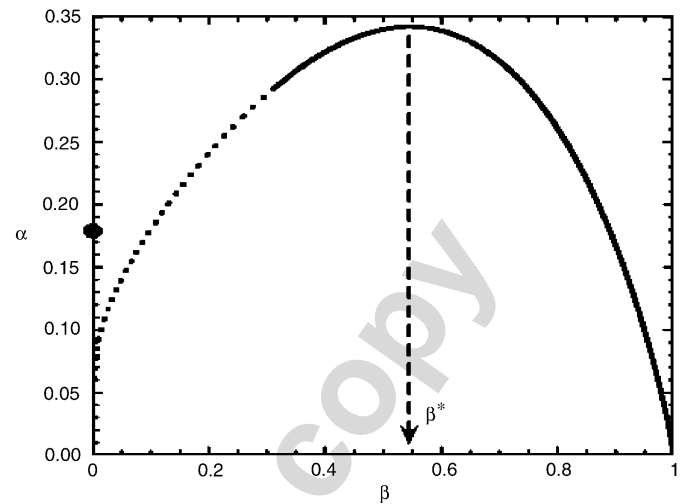


Fig. 4. Function $\alpha(\beta)$ defining the transition condition from the phase diagram of a long nanotube ($\gamma \gg 1$). The black dot on the ordinate axis represents the exact solution considering the core, that is neglected in the solution given by the continuous curve. The dotted portion here represents the region where deviations due to the effect of the core have a progressive effect towards $\beta = 0.0$.

where $F_{21}[\beta] = F_{21}[-\frac{1}{2}, \frac{1}{2}, 2, \beta^2]$ is a hypergeometric function. Upon numerically solving Eq. (8) for different β values we obtained solutions defining $\alpha(\beta)$.

The plot of this analytic expression goes over the points obtained by numerical solution of Eq. (8). In Fig. 3, we present the transition lines for different values of β , for the non-core condition, obtained from Eq. (9). To the left of each line parallel F state prevails while to the right of the same line the vortex V configuration is more stable. Labelled dots a, b and c in Fig. 3 correspond to the cases of the three hysteresis curves reported in the experimental paper by Nielsch et al. [4] defined by (a) $R = 90$ nm, $H = 60$ μm ; (b) $R = 180$ nm, $H = 60$ μm ; (c) $R = 260$ nm, $H = 12$ μm . These radii must be corrected for the oxidation of the tubes. Since CoO is antiferromagnetic the oxide coating does not contribute to the total magnetization. After taking into account the oxide wall data given in the experimental paper the corresponding β values for samples (a), (b) and (c) are 0.983, 0.994 and 0.993, respectively. This last case (short dotted lines) corresponds to the tube with the largest diameter and is inside the V phase and should have a smaller coercive field. On the contrary (a) is well inside the F phase and should have a larger coercive field. These qualitative observations are in good agreement with the measurements performed by Nielsch et al. [4].

Function $\alpha(\beta)$ is plotted in Fig. 4. Care must be applied in the limits of the interval for β . In particular, when β goes to 1.0 we deal with extremely narrow nanotubes, where eventual surface roughness and thickness irregularities of the nanotubes become important. On the other side, when $\beta \rightarrow 0$ we are approaching the limit of a solid cylinder, where the core becomes important and must be considered to get the solution. Fortunately, a recent study considered the effect of the magnetic core in the case of magnetic

nanocylinders for the vortex state [8]. Then, and using the approximation $\gamma \gg 1$, we can estimate the value of $\alpha(0) = 0.179$, which is shown as a dot on the ordinate axis of Fig. 4. The departure of our treatment from the exact one in this limit allows us to think that the actual curve for $\alpha(\beta)$ begins to depart slightly from the one drawn in Fig. 4 at about $\beta = 0.3$, converging to the value given by the dot as $\beta \rightarrow 0.0$.

The condition for the vortex state is maximized for $\beta = \beta^* = 0.546$, i.e. for this value of β the vortex region in the parameter space increases (see Fig. 3). It is interesting to note that the vortex condition weakens from this point on, both for thicker and thinner nanotubes, although due to different reasons. For thick nanotubes ($\beta < \beta^*$), the amount of magnetic material along the z -axis imposes a parallel state along that direction pretty much in the same way it occurs for solid cylinders [8]. For thin nanotubes ($\beta > \beta^*$), the long-range dipolar interaction leading to the vortex state weakens substantially within the planes perpendicular to the z -axis thus facilitating the parallel ordering imposed by dipolar and exchange interactions along the nanotube. However, the curve is non-symmetric, and it will be even more so when the core is considered. This means that the best condition to have magnetic nanotubes with low coercive fields and large remanent magnetization is for long and very narrow nanotubes. We have to recall that this treatment is valid for non-interacting nanotubes.

3. Concluding remarks

Of the three possible configurations for magnetic phases in nanotubes, the one with magnetization perpendicular to the axis ($F1$) is out of consideration because of the

dimensions of nanotubes reported so far in the literature. Then, there is a competition between a parallel state with magnetization along the axis ($F2 = F$) and a vortex state with magnetic moments perpendicular to the axis (V). The equilibrium condition for these two phases is studied in terms of the geometrical aspects of the particle (normalized to the exchange length L_x): outer radius $r = R/L_x$ in the abscissa and length ($h = H/L_x$) in the ordinate, using the ratio of inner to outer radius (β) as a variation parameter. The result is a line that grows faster with r than with h . The law reproducing this behavior is simply $h = \alpha(\beta)r^3$, where the function $\alpha(\beta)$ can be found from Eq. (9). This exercise leads to the conclusion that there is an optimum for the existence of a vortex state, i.e., the maximum value of α . Within this core-free model, the $\alpha(\beta)$ function exhibits a maximum for $\beta = \beta^* = 0.546$. This represents an optimal situation in the case that low coercive fields are sought. As β departs from β^* the vortex condition weakens and coercive fields increase.

Acknowledgments

This work has been partially supported by Fondo Nacional de Investigaciones Científicas y Tecnológicas (FONDECYT, Chile) under Grant nos. 1050013, 1020993 and 1040354, and Millennium Science Nucleus “Condensed Matter Physics” P02-054F of Chile. CONICYT Ph.D. Program Fellowships, as well as MECESUP

USA0108 project are gratefully acknowledged. One author (EEV) is grateful to the Department of Physics of the University of Santiago de Chile for hospitality and partial support during his sabbatical year.

References

- [1] S.Y. Chou, Proc. IEEE 85 (1997) 652; G. Prinz, Science 282 (1998) 1660.
- [2] J.N. Chapman, P.R. Aitchison, K.J. Kirk, S. McVitie, J.C.S. Kools, M.F. Gillies, J. Appl. Phys. 83 (1998) 5321.
- [3] C.A. Ross, M. Hwang, M. Shima, J.Y. Cheng, M. Farhoud, T.A. Savas, H.I. Smith, W. Schwarzacher, F.M. Ross, M. Redjail, F.B. Humphrey, Phys. Rev. B 65 (2002) 144417.
- [4] K. Nielsch, F.J. Castaño, S. Matthias, W. Lee, C.A. Ross, Adv. Eng. Mater. 7 (2005) 217.
- [5] M. Klaui, C.A.F. Vaz, L. Lopez-Diaz, J.A.C. Bland, J. Phys.: Condens. Matter 15 (2003) R985.
- [6] F.J. Castaño, C.A. Ross, A. Eilez, W. Jung, C. Frandsen, Phys. Rev. B 69 (2000) 144421.
- [7] A. Aharoni, Introduction to the Theory of Ferromagnetism, Clarendon Press, Oxford, 1996.
- [8] P. Landeros, J. Escrig, D. Altbir, J. d’Albuquerque e Castro, P. Vargas, Phys. Rev. B 71 (2005) 94435.
- [9] Y.C. Sui, R. Skomski, K.D. Sorge, D.J. Sellmyer, Appl. Phys. Lett. 84 (2004) 1525.
- [10] The public domain package is available at (<http://math.nist.gov/oommf/>).
- [11] D. Weller, A. Moser, L. Folks, M.E. Best, L. Wen, M.F. Toney, M. Schwickert, J.-U. Thiele, M.F. Doerner, IEEE Trans. Magn. 36 (2000) 10.